Nuclear Inst. and Methods in Physics Research, A 1041 (2022) 167360

Contents lists available at ScienceDirect

Nuclear Inst. and Methods in Physics Research, A

journal homepage: www.elsevier.com/locate/nima

The SINQ gas-jet facility as a source for radionuclides from neutron-induced fission of ^{235}U

Georg Tiebel [a,b], Paul Dutheil [a,c], Rugard Dressler [b], Robert Eichler [b,d], Dominik Herrmann [b], Patrick Steinegger [a,b,*]

[a] Laboratory of Inorganic Chemistry, Department of Chemistry and Applied Biosciences, ETH Zürich, Vladimir-Prelog-Weg 1-5/10, Zürich, CH-8093, Switzerland
[b] Laboratory of Radiochemistry, Nuclear Energy and Safety Division, Paul Scherrer Institute, Forschungsstrasse 111, Villigen PSI, CH-5232, Switzerland
[c] Department of Radiation Safety and Security, Paul Scherrer Institute, Forschungsstrasse 111, Villigen PSI, CH-5232, Switzerland
[d] Department of Chemistry, Biochemistry and Pharmaceutical Sciences, University of Bern, Freiestrasse 3, Bern, CH-3012, Switzerland

ARTICLE INFO

Keywords:
SINQ
U-235
Fission products
Gas-jet
Aerosol transport
Radiochemistry
Carrier-free radionuclides

ABSTRACT

The Swiss Spallation Neutron Source SINQ of the Paul Scherrer Institute provides neutrons via proton-induced spallation reactions in a lead target. Produced neutrons are thermalized and impinge on ^{235}U-targets, enclosed in a three-part chamber assembly, which is located in the inner wall of the SINQ shielding. The thermal-neutron-induced fission products can be readily transported from this chamber assembly to a radiochemical laboratory using the gas-jet technique either with a pure carrier gas or with an aerosol-particle-loaded carrier gas. In the past, mainly radioisotopes of the elements Se, Br, Rb, and Kr were retrieved and used for gas-phase chemistry experiments. Here, we present first experiments after the commissioning of the SINQ gas-jet facility as a source of recoverable, non-volatile and volatile, carrier-free fission products for general radiochemical studies and other applications.

1. Introduction

Radionuclides are routinely used in various fields of science and technology. Examples are cancer diagnostics and therapy, material sciences for characterization purposes (e.g., Mössbauer spectroscopy, as sources or markers [1]), in analytics for the determination of elemental contents, e.g., via neutron activation or for the study of chemical properties in general [2,3]. The availability of a variety of radionuclides is also essential in the field of transactinide-element-related, fundamental research (chemical studies of all elements with $Z \geq 104$) in order to develop and benchmark experimental approaches with their lighter homologs [4]. Therefore, an easy and continuous access to a diverse portfolio of carrier-free radioisotopes of different chemical elements is of interest. In particular, nuclear fission represents a feasible way to obtain carrier-free radionuclides in the form of fission products (FPs) suitable for a variety of purposes.

Neutron-induced fission of, e.g., ^{233}U, ^{235}U or ^{239}Pu, is a well-studied process [5] and finds its obvious application in nuclear power generation. Nuclear fission occurs, e.g., after thermal neutron capture, yielding light and heavy fission fragments [6]. In this process a total energy of ≈170 MeV is released together with several neutrons [7]. Neutron-induced asymmetric fission of ^{235}U (as used in the herein presented experiments) was studied comparatively early on and the fission-fragment mass distribution was described already in [8]. The latter is characterized by a double-hump distribution around mass numbers 90 and 140, which is a result of the shell structure of the produced nuclei. The two maxima of the distribution indicate the center of the lighter FP peak (lighter FPP) and of the heavier FP peak (heavier FPP). Due to the conservation of energy and momentum during the fission process, the total energy release is split in such a way, that the isotopes of the lighter FPP obtain a higher kinetic energy than the isotopes of the heavier FPP.

In order to make the produced FPs available for experiments, an adequate coupling between the production site and a radiochemical laboratory is required. For this, a suitable approach is the application of a gas-jet, which was originally introduced by Wollnik and colleagues [9] in 1976 and is still used today [10]. It shall be noted, that herein after the term "gas-jet" refers to systems employing pure carrier gases as well as aerosol-particle-loaded carrier gases for the transport of radionuclides. In an initial step of the herein presented setup, the nuclear reaction products (i.e., the FPs) are stopped and thermalized in an appropriate gas after recoiling out of the thin ^{235}U-targets. Aside from the readily transported volatile fraction of FPs (e.g., Xe), the transport of radioisotopes of non-volatile chemical elements occurs via the addition of aerosol particles to the carrier gas. The aerosol particles act as vehicles onto which non-volatile radionuclides adsorb.

* Corresponding author at: Laboratory of Radiochemistry, Nuclear Energy and Safety Division, Paul Scherrer Institute, Forschungsstrasse 111, Villigen PSI, CH-5232, Switzerland.
E-mail address: patrick.steinegger@psi.ch (P. Steinegger).

https://doi.org/10.1016/j.nima.2022.167360
Received 8 April 2022; Received in revised form 28 July 2022; Accepted 30 July 2022
Available online 13 August 2022

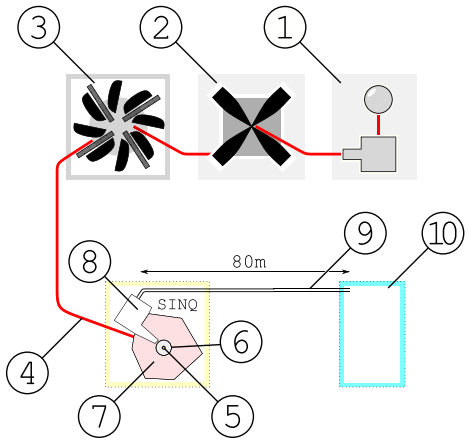

Fig. 1. Overview of the High Intensity Proton Accelerator facility (HIPA) and the Swiss Spallation Neutron Source SINQ at PSI together with the SINQ gas-jet installation. The HIPA facility consists of three cascading accelerators, namely a Cockcroft–Walton accelerator (1), the Injector-2 cyclotron (2) and the ring cyclotron (3); these provide a ≈590 MeV proton beam (4), which is eventually stopped in the SINQ target (5). The spallation-produced neutrons are thermalized in the heavy water moderator (6) surrounded by the stainless steel and concrete biological shielding (7). The gas-jet target assembly is located within this shielding inside the sector 60 insertion module (8), which is connected by 80 m-long capillaries (9) to the radiochemical lab (10).

Depending on the intended experiment, a variety of aerosol materials can be employed for this purpose: For example, KCl can be used to generate soluble aerosol particles with a transportable size distribution between 60 nm to 100 nm [11].

The first gas-jet system, used at the Paul Scherrer Institute (PSI) for FPs, was the SAPHIR gas-jet system, introduced by Nai-Qi et al. [12] in 1989. The system was installed on an external beamline of the SAPHIR research reactor and was also used for preparatory studies with niobium radioisotopes as surrogates for dubnium (Db, $Z = 105$) [12]. After the decommissioning of SAPHIR at the end of 1993, the used ^{235}U-targets were transferred to the then newly built Swiss Spallation Neutron Source (SINQ) to ensure further access to FPs for radiochemical investigations at PSI. Driven by the 590 MeV proton beam of the High-Intensity Proton Accelerator (HIPA) facility, the SINQ at PSI has provided ever since its installment neutrons originating from high-energy proton-induced spallation in a lead target. The neutron spectrum at the position of the ^{235}U-targets, located in the inner shielding of SINQ, is largely dominated by thermal neutrons, thermalized by the heavy water moderator surrounding the SINQ target. The initial neutron flux with a thermal equivalent of $\approx 10^{14}$ cm^{-2} s^{-1} mA^{-1} at the spallation target [13] is reduced to $\approx 10^{9}$ cm^{-2} s^{-1} mA^{-1} at the position of the target chambers [14]. This results in an average FP rate of $\approx 2 \cdot 10^{7}$ s^{-1} mA^{-1} for the entire target assembly.

The first studies conducted at the SINQ gas-jet facility were atmospheric chemistry-related experiments [15,16]. Since only volatile species were targeted during these studies, aerosol-particle-loaded carrier gases were not used. Instead, reactive gases such as carbon monoxide were added to the helium carrier gas in order to promote chemical reactions of the FPs. In these studies, chemical compounds containing radioisotopes $^{83-87}$Se as well as their corresponding bromine daughters were investigated. With the emerging access to FPs from the spontaneous fission of ^{252}Cf through the fission source "Miss Piggy" [17] at the University of Bern, the SINQ gas-jet facility at PSI stopped being used in 2002. The easier and constant access to FPs from ^{252}Cf was accompanied by additional hardware problems at the SINQ gas-jet installation itself. However, a recently finished and extensive upgrade of the control system as well as the exchange of almost all not activated hardware components, has allowed to relaunch experiments at this facility.

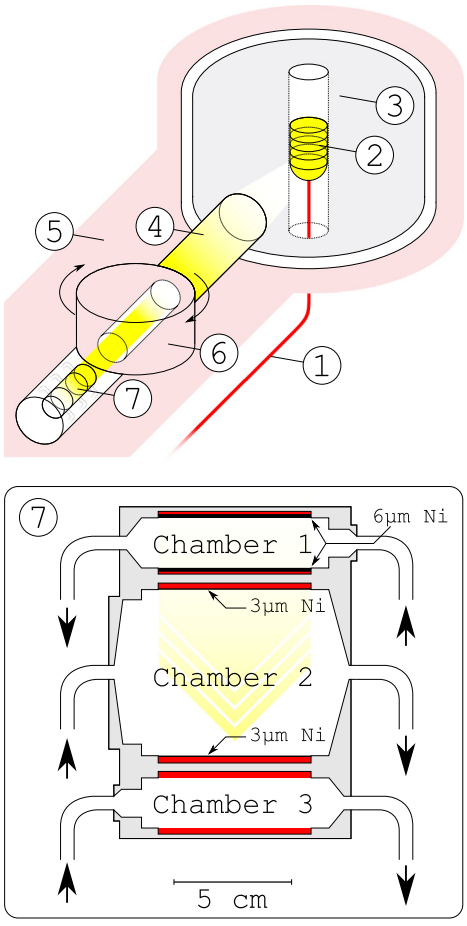

Fig. 2. Scheme of the ^{235}U-target assembly of the SINQ gas-jet facility in the sector 60 insertion module of the Swiss Spallation Neutron Source SINQ at PSI under irradiation with thermal neutrons. The proton beam (1), provided by the HIPA facility (see also Fig. 1), impinges on the SINQ spallation target (2); the resulting neutrons (yellow) are largely thermalized in the heavy water moderator tank (3) and can subsequently exit through a dedicated beamline (4) to the target chamber, located in the inner biological shielding (5) with the shutter (6). The latter controls the neutron flux on the target assembly (7): If the shutter is open, the ^{235}U-target chamber assembly is exposed to neutrons, thus leading to recoiling fission products; these can be mobilized by means of the (aerosol-particle-loaded) carrier gas. The enlargement shows the three cylindrical chambers with individual indications for the entering and exiting carrier gas flow (black arrows), the ^{235}U-targets (red) as well as the nickel degrader foils (black).

Here, we present the results from the recommissioning of the SINQ gas-jet facility. This work aims at establishing a radionuclide inventory in dependence of the used transport method, i.e., an inert gas versus an aerosol-particle-loaded carrier gas transport, as well as of the experimental conditions and the measurement procedure. The results will serve as a basis for future radiochemical experiments with the determined radionuclides at carrier-free amounts. Furthermore, the influence of originally included Ni degrader foils on top of some of the ^{235}U-targets are addressed.

2. The SINQ gas-jet facility

The SINQ gas-jet system is located at the Swiss Spallation Neutron Source (SINQ), which is driven by the high-intensity, high-energy proton beam of the HIPA facility (see Fig. 1). The following subsections describe the individual parts of SINQ gas-jet system.

2.1. The ^{235}U-target assembly

Located in the sector 60 insertion module of the SINQ, a three-part ^{235}U-target chamber assembly is installed (Fig. 2). The target assembly

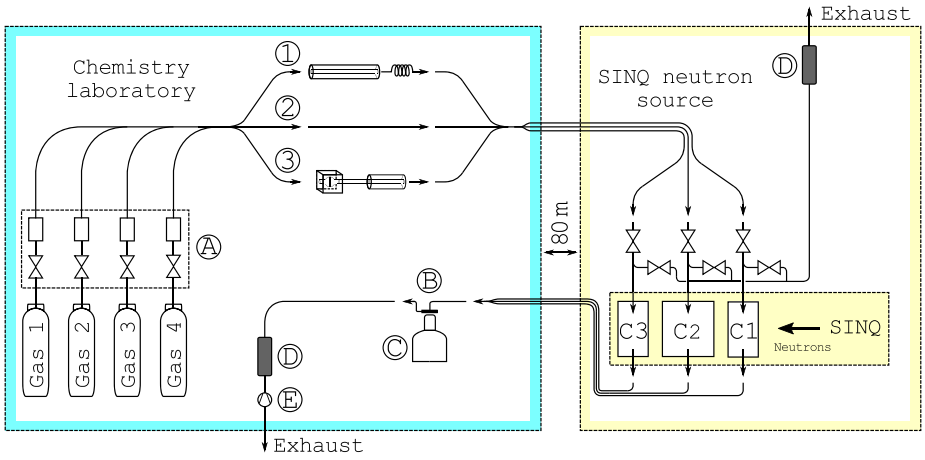

Fig. 3. The gas-jet transport system spanning between the radiochemical laboratory (framed in turquoise) to installations at the Swiss Spallation Neutron Source SINQ (framed in yellow; for a detailed chamber description, see Fig. 2) with (A) the carrier gas supply system with electromagnetic valves and mass flow controllers for carrier gas mixtures of up to four gases, (B) the collection point for the fission products (FPs), (C) the HPGe γ-detector, (D) large-capacity, activated charcoal traps at the exhaust, and (E) the backing pump. The transport modes of FPs are (1) the salt-aerosol generator using a tubular furnace, (2) a pure carrier gas, and (3) the spark-discharge aerosol generator; at position (B), aerosol-particle-loaded carrier gases (non-volatile FPs) are passed over a glass-fiber filter, while pure carrier gases (volatile FPs) are retained in an activated charcoal trap.

is placed behind a remotely controlled neutron shutter on the outer wall of the SINQ moderator tank. Two ^{235}U-targets are mounted on opposite walls in each cylindrical chamber (i.e., six targets in total). All chambers have a 70 mm inner diameter. Whereas, chambers 1 and 3 are 25 mm long, the central chamber 2 has a length of 70 mm. Each chamber has one inlet and one outlet tube (both made of anodized aluminum) with a dimension of 4 mm × 2 mm (outer × inner diameter), which are directly welded-in on opposite sides of the chamber. Aluminum was chosen to limit long-lived neutron-activation products within the target assembly itself. The inlet and outlet capillaries can be connected on the outside of the SINQ insertion module to two types of transport lines (i.e., stainless steel or polyethylene tubing), which link the production site to the radiochemical laboratory.

The ^{235}U-targets were prepared by molecular electroplating with surface densities between 80 $\mu g\,cm^{-2}$ and 180 $\mu g\,cm^{-2}$ of highly enriched ^{235}U (enriched to 99.7 %) on 62(2) mm circular aluminum backings. In total, 21.76 mg ^{235}U were used for all targets. Nickel foils were placed onto all targets in chambers 1 and 2, while the two targets in chamber 3 remained uncovered. The purpose of the nickel degrader foils was the potential suppression of isotopes of the heavier FPP in favor of the lighter FPP (a hypothesis tested in the herein presented experiments). While the two targets from chamber 1 were covered by 6 μm thick Ni foils, the two targets in chamber 2 were covered with 3 μm thin foils of Ni.

A neutron shutter separates the ^{235}U-target assembly from the SINQ target in ≈2.5 m distance (Fig. 2). The shutter with a central opening consists of an aluminum drum filled with boron carbide (with boron featuring a high cross section for (n, α)-reactions and thermal neutrons), whereas the remaining neutron shielding is made of high-purity stainless steel. The cylindrical hole in the shutter has a diameter of ≈6 cm. Thus, a fully opened drum shutter allows for a full "illumination" of the entire diameter of the target assembly by the incoming neutron beam. Moreover, the opening angle of the shutter is fully adjustable and can be remotely controlled from the laboratory by means of the gas-jet control system. This allows the operator to gradually reduce the neutron flux [18]. Fission rates of up to ≈$8\cdot10^{6}$ s^{-1} per ^{235}U-target can be reached with a 1 mA proton beam on the SINQ target. When fully closed, the shutter reduces the neutron flux by a factor of about 150 [14].

2.2. The gas-jet transport system

The general layout of the gas-jet transport system is depicted in Fig. 3. A setup of electromagnetic valves and mass flow controllers, located in the radiochemical laboratory and connected to a central control system (see Section 2.3), are used to define and activate user-specific gas flow parameters at the beginning of each experiment. In that way, a mixture of up to four different carrier gases can be established. The gas-jet system allows for pressures of up to 2 bar (alarm at 1.5 bar and interlock at 2 bar; mass flow rates up to 1.5 L min^{-1} depending on the used gas or gas mixture). The pressure-driven carrier gas (mixture) reaches the target chamber assembly (note that the SINQ is located in an adjacent building) through 80 m stainless steel capillaries (6 mm × 4 mm). An individual chamber inlet has to be opened by electromagnetic valves beforehand (one chamber at a time). Afterwards, the stopped and mobilized fraction of FPs is transported back to a collection point in the radiochemical laboratory. The outlet transport lines of the target chambers can be changed between stainless steel or polyethylene (4 mm × 2 mm). The smaller inner diameter allows for a faster transport and thus, for a higher yield of short-lived FPs. The transport time based on plug flow conditions between the target chambers and the laboratory is estimated to be about 22 s at a flow rate of 0.7 L min^{-1}. Including the volume of the target chambers, the transport time increases to roughly 30 s in the case of chamber 1 or 3 and to 46 s for chamber 2. A pump was placed at the exhaust of the circuit after the collection point to adjust the pressure gradient in the system.

So far, two different types of aerosol generators can be included in the gas-jet circuit to transport non-volatile radionuclides (see Fig. 3). The salt-aerosol generator consists of a tubular furnace, hosting a stainless steel tube into which a ceramic boat, loaded with the desired salt (usually KCl), can be placed. Upon heating the boat to >650 °C, aerosol particles are generated [12] and transported with the carrier gas downstream to the target assembly. The second option regarding aerosol generation is a spark discharge generator, which can be used to produce non-soluble carbon or metal aerosol particles. An applied potential difference of up to 10 kV between opposite electrodes, made of the material from which the aerosol particles are to be generated, triggers a discharge with a frequency of about 5 Hz. Both approaches lead to a particle number concentration of at least 10^{13} cm^{-3}. Aerosol particles with a mobility-diameter of around 100 nm, as obtained with these two approaches, are transported with high yields to the target chambers. Therein the thermalized, non-volatile FPs adsorb onto the surface of the aerosol particles and thus, can be transported to the radiochemical laboratory [9].

In the laboratory, the volatile FPs are typically accumulated using activated charcoal traps, whereas the non-volatile fraction of FPs can be collected by passing the aerosol-particle-loaded carrier gas through

glass fiber filters. These filters retain all aerosol particles and thus, all non-volatile species. The volatile fraction of FPs, which does not adsorb on the surface of the aerosol particles, passes through and is retained on another, subsequently placed charcoal trap. The decay of transported FPs in both traps can be monitored by placing them directly in front of a HPGe (high-purity germanium) γ-detector.

2.3. Control system and safety monitoring

The SINQ gas-jet control system regulates and monitors all components (e.g., pressure gauges and mass flow controllers) and ensures safe operation within the framework of predefined interlock criteria (e.g., maximum pressures in the target chambers, thresholds of the dose rate and more). It is based on SIMATIC programmable control units (Siemens) being driven and/or read out by a tailored software solution (PSI in-house development). This allows users to setup and run their experiments from the radiochemical laboratory in a fully automated way. Keeping exposure to radioactivity low and avoiding contamination are prerequisites for a safe operation and must be ensured at all times. Thus, several safety features have been implemented in that respect. On the one hand, the exhaust gas is filtered through a large-capacity activated charcoal cartridge at the exhaust of the transport system to ensure that no radionuclides are released into the central venting installation. Furthermore, to avoid an uncontrolled release in case of ruptured tubing, all capillaries of the gas flow circuit are placed in cladding tubes, while the gas-extraction points in the chemical laboratory are kept in an air-tight box. The interstitial air from the gas-purged cladding tubes as well as from the air-tight boxes is subject to constant radioactivity monitoring and is continuously exchanged by pumping it away through additional activated charcoal cartridges. The proton beam intensity from the HIPA facility (which is proportional to the neutron flux received on target), as the only external parameter, has been directly embedded in the control software and can be retrieved from the SINQ database system.

3. Experimental

To qualitatively characterize the SINQ gas-jet system, the transport of volatile FPs from all three chambers was explored using a 9:1 (volume ratio) He/N_2 carrier gas mixture (with one exception; imposed radiation protection measures, prevented the extensive use of Ar in the experiments described here). To demonstrate the full inventory of accessible FPs, chamber 2 was operated with He/N_2 and Ar/N_2 carrier gas mixtures, loaded with KCl aerosol particles. These were chosen to exploit the different stopping behavior of FPs in these gas mixtures. Two experimental parameters were kept constant at all times in order to achieve comparable experimental conditions:

- The **gas flow rate** as an important parameter, mainly determining the transport efficiency of short-lived FPs to the radiochemical laboratory.
- The **pressure** in the chambers affecting the stopping behavior of the FPs was adjusted accordingly to maintain a chamber pressure in the range of 1.4 bar to 1.5 bar.

The experimental conditions of all conducted experiments are compiled in Table 1. The neutron beam shutter was fully opened during all experiments. In the case of the experiments with pure gases only, the transported, volatile fraction of FPs (see Section 5.1) was collected on an activated charcoal trap (trapping efficiency close to 100 % verified by non-measurable amounts in a subsequent charcoal trap), placed directly in front of a HPGe γ-detector (ORTEC GEM 13180 SV, with 13.1 % relative efficiency and a resolution of 1.68 keV at 1.33 MeV). For each of the conducted experiments, γ-spectrometric measurements were performed during the roughly two-hour-long collections as well as 12 h after the end of the corresponding experiment (t_{live} = 2 h for the offline measurement of long-lived FPs). For the experiments employing a KCl-aerosol-particle-loaded carrier gas, the oven, containing the crucible with KCl, was heated to an operating temperature of 650 °C to 675 °C. The thus generated aerosol particles allowed for the transport to and the collection of non-volatile FPs (see Section 5.2) on glass fiber filters, which were mounted in a dedicated holder in front of the HPGe γ-detector. As in the case of the experiments with the volatile FPs, γ-spectrometric measurements were recorded during the roughly 2 h collection periods. These were likewise followed by a second γ-spectrometric measurement, conducted 24 h after the end of collection (t_{live} = 2 h for the offline measurement of long-lived FPs). All measured γ-spectra were controlled and evaluated using the Genie 2000 software suite [19].

Table 1
Summary of the experimental conditions of all conducted experiments.

Chamber	Gases	Flow rate [L min^{-1}]	Pressure [bar]	KCl aerosol (temperature) [°C]	Effective sampling time [s]
1	He/N_2	0.7	1.45(1)	no	7453
2	He/N_2	0.7	1.40(3)	no	7739
2	He/N_2	0.7	1.39(1)	yes (675)	7597
2	Ar/N_2	0.7	1.49(1)	yes (675)	8012
3	He/N_2	0.7	1.44(1)	no	7978

4. Simulations with SRIM

For a comparison with the experimental results, simulations with SRIM were carried out [20]. To account for the random spatial occurrence of neutron-induced fission events in the ^{235}U-targets, a specific input file was generated. For this, the ^{235}U-atoms were uniformly distributed over the target area as well as the target thickness of about 90 nm. The emission direction of the FPs was homogeneously distributed into the target chamber volume. The kinetic energies of simulated ions were randomized (normally distributed random values) according to values given in [21]. The thus generated input for SRIM comprised information on the individual starting positions, the emission angles, as well as the kinetic energies for 10 000 ions.

For the simulations, a density of $3.75 \cdot 10^{-4}$ g cm^{-3} (p = 1.45 bar) was used for the He/N_2 gas mixture (9:1), assuming ideal gas behavior. Furthermore, a correction factor of 1.4 was included, which accounts for the overestimation of the stopping force in gases by SRIM [22]. Multiple simulations for two different isotopes, namely ^{89}Kr and ^{138}Xe, were carried out. A radial-depth distribution was obtained by binning the endpoints of the trajectories on a 4 mm × 2 mm grid. The results of these simulations are presented in Fig. 4 for ^{89}Kr (as a member of the light FPP) and ^{138}Xe (as a member of the heavy FPP) together with rectangular enclosures, illustrating the two chamber sizes (black, solid frame for chambers 1 & 3 and black, dashed frame for chamber 2). Based on these simulations, we note the following:

- In case of chamber 1 (6 µm Ni foil; solid, green contour line and solid, black frame) a large fraction of the ^{89}Kr ions is stopped within the chamber, whereas no ^{138}Xe passes through the 6 µm Ni foil (straight solid, green line at a depth of 0 mm).
- In case of chamber 2 (3 µm Ni foil; dashed–dotted, blue contour lines and dashed, black frame) a little less ^{89}Kr is stopped within the chamber in comparison with ^{138}Xe.
- In case of chamber 3 (no Ni foil; dashed–dotted–dotted, red contour lines and solid, black frame) most FPs (heavy and light) should predominantly implant in the chamber walls; heavier a little less than lighter ions.

The experimental results and simulations are only qualitatively comparable, as it is known that SRIM has some limitations, especially for the description of the stopping of ions in gases [22,23]. As found in [24], simulations of the stopping behavior of ions in gases with the

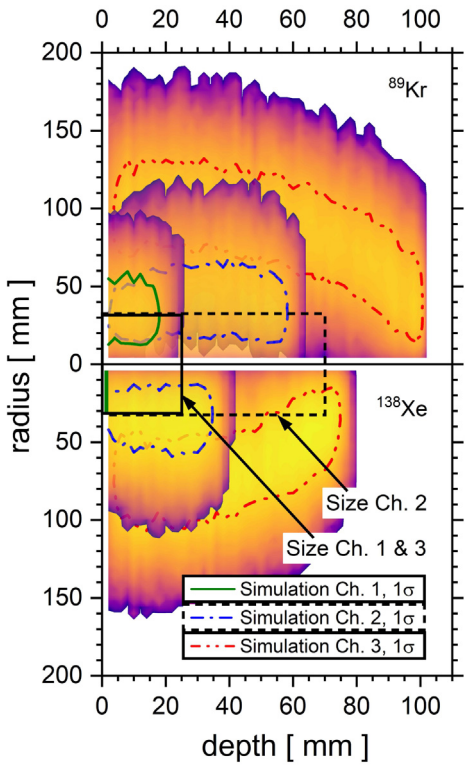

Fig. 4. Radial-depth distribution of fission products (color scale indicates number density from low [violet] to high [yellow] covering four orders of magnitude in arbitrary units) as result of six SRIM simulations (i.e., two isotopes and three target settings) for all three chambers (chamber 1 with 6 μm Ni, chamber 2 with 3 μm Ni, and chamber 3 without a Ni degrader), a He/N_2 gas mixture (9:1) as well as using the radionuclides ^{89}Kr and ^{138}Xe as representatives of the light fission product peak and the heavy fission product peak; the contour lines indicate the stopping region of 68.27 % (1σ) of FPs (note here: the full stopping of ^{138}Xe in the 6 μm Ni degrader foils of chamber 1 is indicated by a green line at a depth of 0 mm), whereas the chamber sizes are shown as superimposed frames (solid, black frame for the size of chambers 1 & 3 and the dashed, black frame for the size of chamber 2).

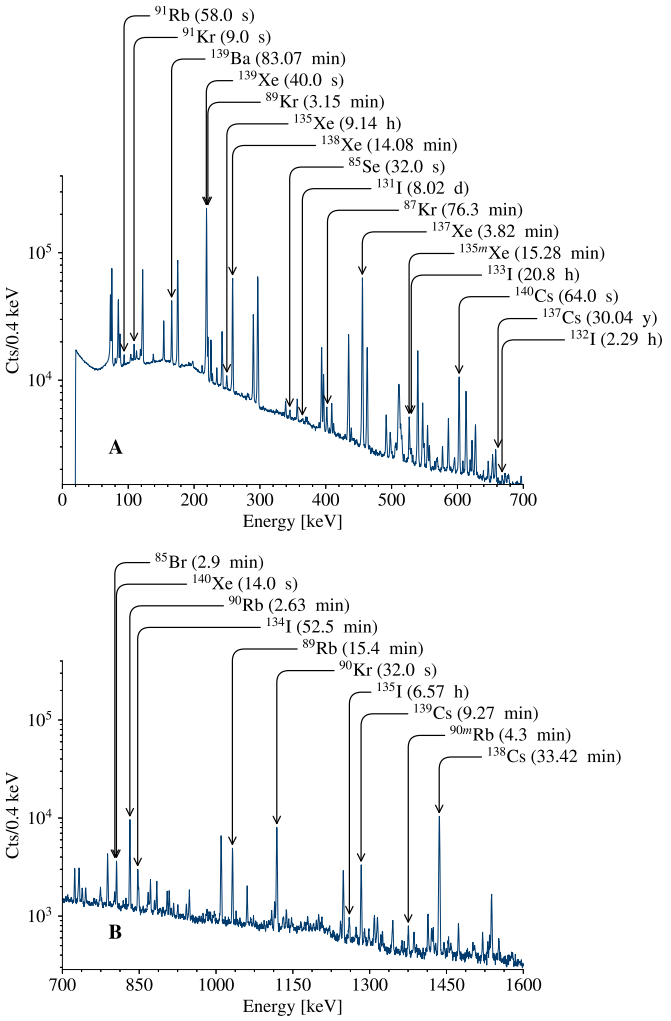

Fig. 5. γ-spectrum (t_{live} = 7200 s; measured during collection) of short-lived fission products, as transported from within chamber 2 with a pure He/N_2 (9:1) carrier gas mixture (0.7 L min^{-1}) to an activated charcoal trap; identified radionuclides are shown for the γ-energy range of (A) 20 keV to 700 keV and (B) 700 keV to 1600 keV; background peaks are not labeled.

help of SRIM may deviate from experiments by up to a factor of 4. Furthermore, Sigmund and colleagues [23] report on discrepancies of SRIM data even for the solid phase. These observations in combination with our experimental results as well as uncertainties regarding the target setup and installation roughly 30 years ago (e.g., uncertainties of foil thicknesses), prevent a one-to-one quantitative comparison.

5. Results and discussion

The thermal neutron-induced fission of ^{235}U and its resulting FPs are well known [8]. Since a variety of different radionuclides is produced, the resulting γ-spectra are complex, which complicates the data evaluation (e.g., because of superimposed γ-lines). Thus, in the displayed spectra, for reasons of simplicity, it was decided to label only the major line of each identified radionuclide. The remaining lines are either superpositions of several smaller lines or belong to a radionuclide, whose main γ-line is more intense. Many radionuclides were successfully identified and a corresponding inventory of easily accessible radionuclides has been established. For an even more detailed analysis, radiochemical separations could be performed prior of the γ-spectrometric measurements.

5.1. Experiments with pure gases

Since the highest isotopic variety of FPs from both, the lighter as well as from the heavier FPP is expected for chamber 2 (i.e., chamber with the largest depth as well as a 3 μm thin Ni degrader foil), the latter was used for the evaluation of the accessible radionuclide inventory (see Fig. 5). The identified radionuclides in the recorded γ-spectra for a transport by a pure He/N_2 carrier gas mixture, expectedly shows that only volatile FPs reach the radiochemical laboratory. Radioisotopes of the noble gases Kr and Xe, but also Br or I are particularly noteworthy. Likewise identified non-volatile species (e.g., ^{91}Rb or ^{139}Cs) are exclusively daughters of transported volatile FPs.

To probe the influence of the three different target setups (i.e., the chamber sizes as well as the different Ni degrader foils and no coverage) on the stopping and transport of differently heavy FPs, two volatile FPs (i.e., elements with negligible retention loss during transport) with adequate half-lives were evaluated. In order to determine relative yields for both FPPs, the γ-spectra, recorded during collection, were analyzed for the peak areas of the main γ-lines of ^{89}Kr ($t_{1/2}$ = 3.15(4) min [25], representative of the lighter FPP) and ^{138}Xe ($t_{1/2}$ = 14.08(8) min [26], representative of the heavier FPP). To this end, the corresponding peak areas of the main γ-line of each radionuclide (E_γ[^{89}Kr]=220.948(9) keV [25] and E_γ[^{138}Xe]=258.411(20) keV [26]) were normalized to the measurement time as well as the fission yields (^{89}Kr 4.511(63) %; ^{138}Xe 6.297(88) % [27]) and corrected with a factor f_{grow} in order to take the in-growth and decay during collection into

Table 2
Summary of the results from three different collections/γ-spectrometric measurements (three chambers, pure He/N_2 carrier gas) regarding the transport of ^{89}Kr and ^{138}Xe as exemplary volatile fission products from the lighter and heavier fission product peak; the evaluated isotope ratio corresponds to the ratio of ^{89}Kr/^{138}Xe.

Radionuclide	Live time	Count rate	Isotope ratio	
	[s]	[cts s^{-1}]	Experiment	SRIM
Chamber 1 (small, 6 µm Ni)				
^{89}Kr ^{138}Xe	6898	425(23) 152.3(96)	2.00(17)	≫1
Chamber 2 (large, 3 µm Ni)				
^{89}Kr ^{138}Xe	7200	2550(130) 16100(840)	0.1133(85)	≈1
Chamber 3 (small, no Ni)				
^{89}Kr ^{138}Xe	7300	837(42) 7850(400)	0.0764(56)	0.2

account (Eq. (1) taken from [19]):

$$f_{grow} = 1 - \frac{1 - \exp\left(-\lambda \cdot t_{live}\right)}{\lambda \cdot t_{live}} \quad (1)$$

where λ is the decay constant, corresponding to $\lambda = \ln(2)/t_{1/2}$. From this, the isotope ratios of ^{89}Kr/^{138}Xe were calculated (see Table 2). The highest yields of radionuclides from the heavier FPP (i.e., isotope ratios ^{89}Kr/^{138}Xe < 1) were observed in case of chambers 2 and 3 (see Table 2). This is a consequence of the higher kinetic energy of the FPs from the lighter FPP and the thereof resulting longer stopping range. Thus, the likelihood for these FPs to collide with the walls or the opposite target is higher in comparison to the FPs belonging to the heavier FPP. In contrast to that, the targets in chamber 1, both being covered with a 6 µm Ni foil, led to an isotope ratio ^{89}Kr/^{138}Xe >> 1. Hence, radionuclides of the lighter FPP are dominating, whereas a larger part of the FPs from the heavier FPP was fully stopped within the thick Ni degrader foils (see Table 2). These observations are in general agreement with the trends from the simulations with SRIM (see Section 4 and the isotope ratios given in Table 2). Although predicting for chamber 1 that no ^{138}Xe penetrates the 6 µm thick degrader foil, the radioisotope was observed nonetheless during the conducted experiments. Besides the overall limited information regarding the actual target installation in 1993, the experimental observation may be further explained by thickness variations of the degrader foils (e.g., *Goodfellow* states variations of ±25 % for their 3 µm and 6 µm Ni foils) as well as predictive limitations of SRIM itself [23,24].

Generally the highest transported amounts of ^{89}Kr and ^{138}Xe were obtained for chamber 2 (see Table 2). Therefore, this chamber served as reference for the following evaluation. Since chamber 2 is the deepest chamber (i.e., 70 mm) and features the thinner Ni degrader foils, overall more FPs are expected to be stopped in the carrier gas instead of being implanted in the chamber walls or in the opposite target (see Section 4). As the isotope ratio ^{89}Kr/^{138}Xe is similar to the one obtained for chamber 3 without any target coverage, the influence of the 3 µm Ni degrader foil seems of minor relevance for the preferential selection of one or the other FPP. The difference in yields between chambers 2 and 3 results from the different chamber depths. ^{89}Kr was obtained with a relative yield (in comparison to the result for ^{89}Kr from chamber 2) of 32.9(23) %, while for ^{138}Xe a relative yield of 48.8(36) % was determined. In case of both chambers, a larger part of FPs of the lighter FPP impinges into the walls due to the higher kinetic energies. This effect is even more pronounced for the smaller chamber 3 with a depth of only 25 mm. Thus, ^{89}Kr and other radionuclides of the lighter FPP are generally transported with lower relative yields from chambers 2 and 3 than radionuclides from the heavy FPP, with a pronounced decrease in case of chamber 3 due to its smaller dimensions. This experimental observation is backed by the trends retrieved from simulations with SRIM (see Fig. 4).

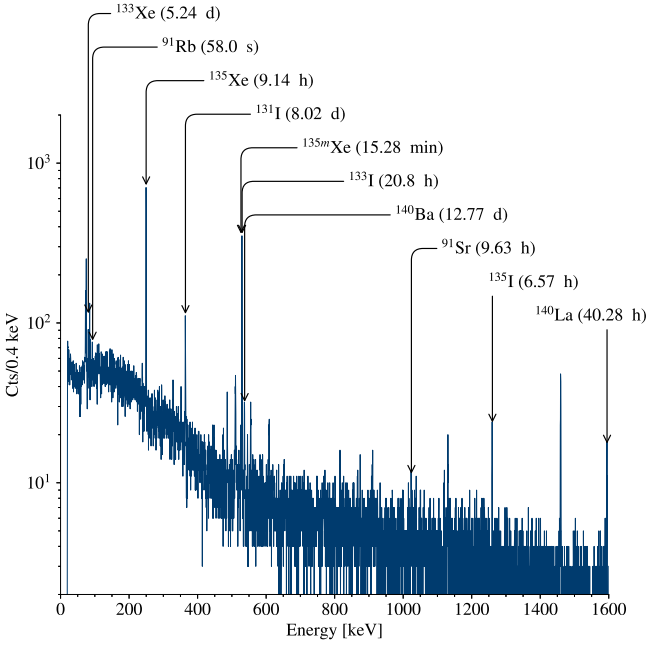

Fig. 6. γ spectrum (t_{live} = 7200 s) of long-lived daughter nuclides of initially transported short-lived fission products or long-lived fission products directly transported from within chamber 2 with a He/N_2 (9:1) carrier gas mixture, as measured after 12 h after the end of collection; background peaks are not labeled.

The lowest amounts of transported FPs were obtained for chamber 1. The relative yields (in comparison to the results from chamber 2) amount to 16.7(12) % for ^{89}Kr and only 0.946(77) % for ^{138}Xe. This is a consequence of a larger fraction of heavier FPs being fully stopped in the roughly 6 µm thick Ni foils (i.e., higher atomic number/mass leads to a lower kinetic energy). Meanwhile, a still considerable amount of FPs of the light FPP implant in the walls or opposite targets due to the relative small chamber depth of only 25 mm.

12 h after the end of collection, only longer-lived radionuclides remain in the charcoal trap (see Fig. 6). These are either directly transported, long-lived and volatile FPs or their daughters (e.g., ^{135}I with $t_{1/2}$ = 6.58(3) h and ^{135}Xe with $t_{1/2}$ = 9.14(2) h [28]) or descendent, long-lived radionuclides of short-lived and volatile FPs (e.g., ^{140}Xe with $t_{1/2}$ = 13.6(1) s and its granddaughter ^{140}Ba with $t_{1/2}$ = 12.7527(23) d [29]).

5.2. KCl-aerosol experiments

The identification of radionuclides transported with an aerosol-particle-loaded carrier gas is more complex due to the wider variety of transported radioisotopes of multiple chemical elements. Mainly radioisotopes of less-volatile elements were detected at the collection site. The more volatile fraction of FPs (e.g., ^{134}I or ^{135}Xe) passed predominantly through the glass fiber filter and were transported further downstream to a secondary charcoal trap. Thus, volatile FPs are largely suppressed in the corresponding γ-spectra. For reasons of clarity and in agreement with the approach pursued earlier, only one radioisotope per identified element is marked in the spectra shown below (see Fig. 7).

The isotope ratios of a representative of the lighter FPP (i.e., ^{84}Se, $t_{1/2}$ = 3.26(10) min [30]) and the heavier FPP (i.e., ^{134}Te, $t_{1/2}$ = 41.8(8) min [31]) were evaluated regarding the transport yields with a He/N_2 as well as a Ar/N_2 carrier gas mixture. In order to do so, the peak areas of two clearly distinguishable γ-lines of the two radionuclides were evaluated in the corresponding γ-spectra (i.e, E_γ[^{84}Se]= 408.2(4) keV [30] and E_γ[^{134}Te]= 767.20(2) keV [31]). These were then normalized to the measurement time and corrected with the fission yields (^{84}Se 0.966(27) %; ^{134}Te 6.97(20) % [27]) as well as

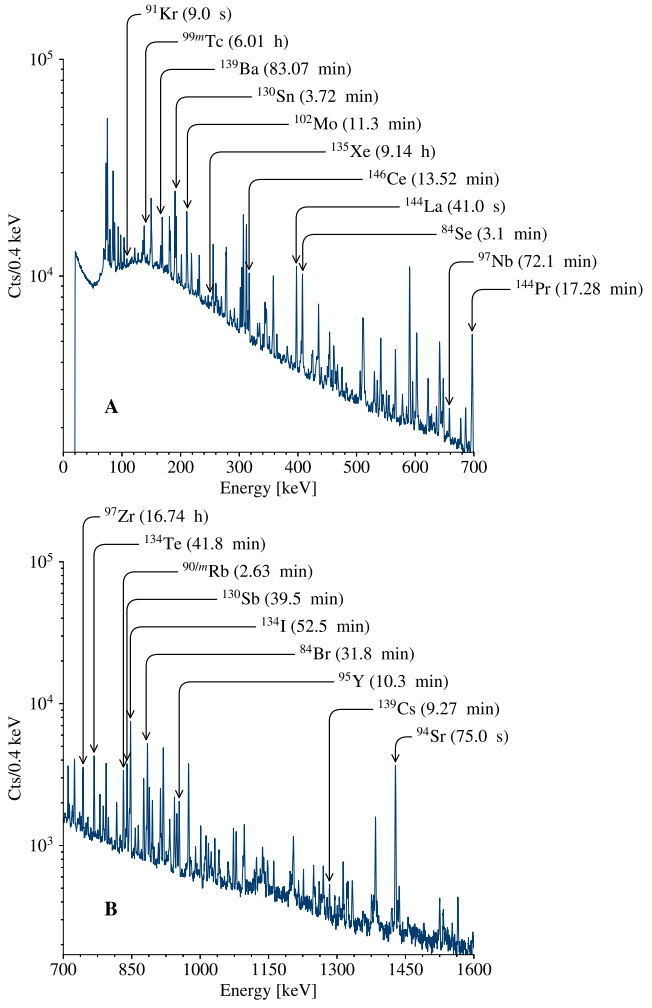

Fig. 7. γ-spectrum (t_{live} = 7200 s; measured during collection) of short-lived fission products, as transported from within chamber 2 with a KCl-aerosol-particle-loaded He/N_2 (9:1) carrier gas mixture (0.7 L min^{-1}) onto a glass fiber filter; identified radionuclides are shown for the γ-energy range of (A) 20 keV to 700 keV and (B) 700 keV to 1600 keV; background peaks are not labeled.

Table 3
Summary of the results from two different collections/γ-spectrometric measurements (chamber 2, two carrier gas mixtures) regarding the transport of ^{84}Se and ^{134}Te as exemplary fission products from the lighter and heavier fission product peak; the evaluated isotope ratio corresponds to the ratio ^{84}Se/^{134}Te.

Radionuclide	Live time [s]	Count rate [cts s^{-1}]	Isotope ratio
He and N_2 (9:1)			
^{84}Se	7200	17.3(11) · 10^3	0.0888(82)
^{134}Te		26.9(14) · 10^3	
Ar and N_2 (9:1)			
^{84}Se	7200	29.6(19) · 10^3	0.985(91)
^{134}Te		4.16(22) · 10^3	

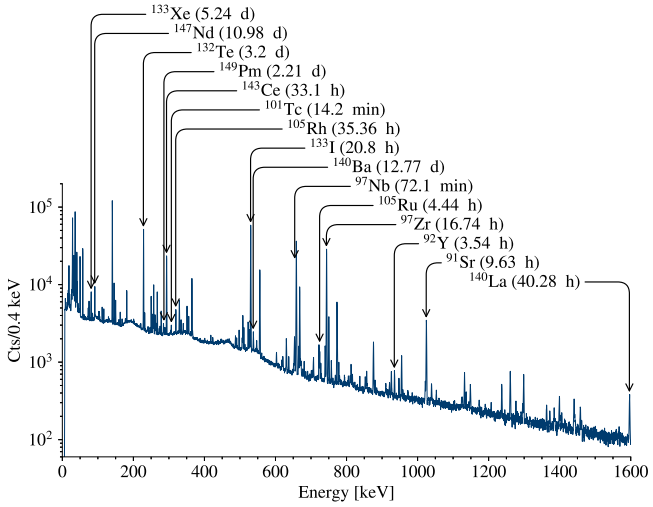

Fig. 8. γ-spectrum (t_{live} = 7200 s) of long-lived daughter nuclides of initially transported short-lived fission products or long-lived fission products directly transported from within chamber 2 with a KCl-aerosol-particle-loaded He/N_2 (9:1) carrier gas mixture as measured 24 h after the end of collection; background peaks are not labeled.

the above-mentioned factor f_{grow} from Eq. (1). The results of both experiments with the two different KCl-aerosol-particle-loaded carrier gas mixtures (see Table 3) were treated in the same way as in case of the pure gas transport (see Section 5.1). A comparison of these experiments with simulations using SRIM is not meaningful, as the aerosol adds an additional degree of uncertainty to the already rather complex problem. Thus, simulations will be even less conclusive than for the volatile FPs. However, the comparison between the two different carrier gas mixtures gives an impression regarding the transport perspectives using gases with higher stopping force, e.g., argon or nitrogen.

The isotope ratio of ^{84}Se/^{134}Te, which is higher by more than a factor of 10 in the case of Ar/N_2 compared to He/N_2, confirms the expected overall better stopping of FPs in the argon-based carrier gas mixture.

The longer-lived radionuclides were likewise identified by a second γ-spectrometric measurement 24 h after the end of collection (see Fig. 8).

6. Radionuclide portfolio

Considering all identified radionuclides, a final portfolio of currently accessible radionuclides can be evaluated (see Figs. 9A and 9B). Since an overall large number of radionuclides were transported, not all accessible radionuclides could be clearly identified and marked in Figs. 9A and 9B. This is a consequence of different fission product yields, decay modes, branching ratios as well as overlapping γ-lines or a superposition of background activity in the corresponding γ-spectra. Further reasons for gaps in the presented radionuclide portfolio concern the scarcity of transport of the parent nuclide or the radionuclide in question itself as well as a lack of γ-lines of the corresponding radionuclide.

7. Summary

The recommissioned SINQ gas-jet facility is a versatile source for a large variety of FPs from thermal neutron-induced fission of ^{235}U. The FPs can be readily transported by the gas-jet technique to the radiochemical laboratory. The recommissioned system has been described and characterized as well as a radionuclide portfolio has been established. A variety of short- as well as long-lived, volatile and non-volatile radionuclides could be identified (see Figs. 9A and 9B). Beside the qualitative analysis in the form of a radionuclide portfolio, the preferential transport of FPs from the light and heavy FPP out of the three chambers was addressed in dependence of the individual chamber setup. Under certain experimental conditions, it was shown that either of them may be preferentially transported. However, these findings are of minor relevance regarding actual experimental implications.

The herein presented results highlight the potential of the SINQ gas-jet facility as a versatile source of neutron-rich, carrier-free radionuclides in Switzerland, which can be used for a wide variety of radiochemical experiments. Subsequent physical or chemical separations may lead to single, radiochemically pure samples of a carrier-free

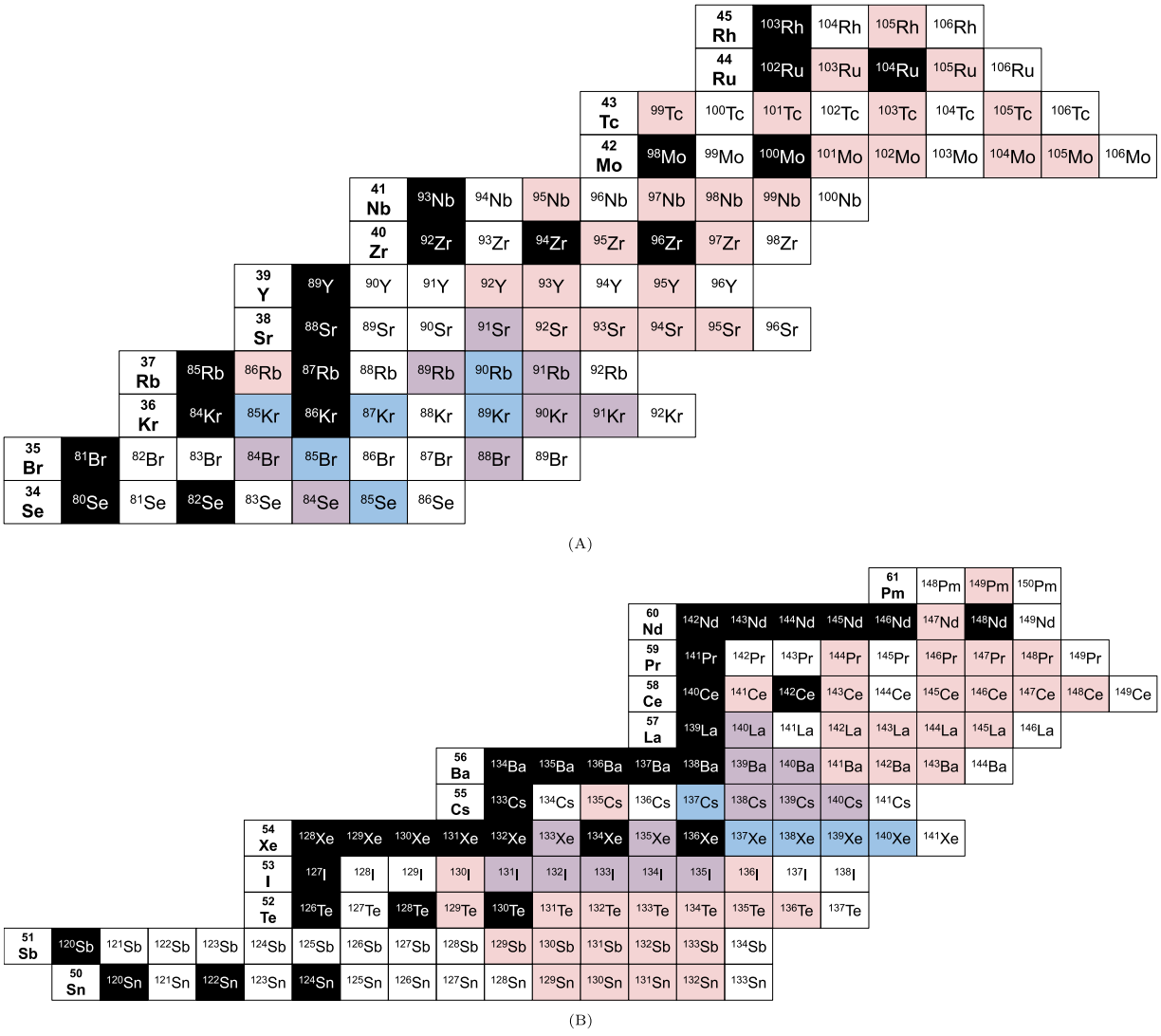

Fig. 9. Excerpt of the chart of nuclides, highlighting all yet identified radionuclides in blue (pure gas transport only), in red (aerosol-particle-loaded carrier gas transport only), and in purple (observed with both transport approaches) as fission products from thermal neutron-induced fission of ^{235}U with (A) the lighter fission product peak, and (B) the heavier fission product peak (stable isotopes are displayed in black).

radionuclide for dedicated investigations. These tracers will be used to perform studies from applied topics all the way to fundamental radiochemical research. First radiochemical studies comprised tests of an innovative whey-based filter material [32]. The transport and collection of a broad portfolio of radionuclides using a KCl-based gas-jet enabled the preparation of aqueous samples containing carrier-free radionuclides. The retention of a broad variety of radioisotopes of various chemical elements on the novel filter material revealed a rather universal applicability with low elemental selectivity [33]. Further developments are currently pursued in the form of, e.g., a continuous transfer of radionuclide-loaded salt aerosols into the liquid phase [34].

Declaration of competing interest

The authors declare that they have no known competing financial interests or personal relationships that could have appeared to influence the work reported in this paper.

Data availability

Data will be made available on request.

Acknowledgments

The authors would like to thank Christoph Stettler (PSI) for the development of the tailored software solution of the SINQ gas-jet control system.

This work was supported by the Swiss National Science Foundation, Switzerland (project grant 200020_196981/1) and the Swiss Federal Nuclear Safety Inspectorate, Switzerland (contract number: CTR00836).

References

[1] M.I. Oshtrakh, V.A. Semionkin, V.I. Grokhovsky, O.B. Milder, E.G. Novikov, Mössbauer spectroscopy with high velocity resolution: New possibilities of chemical analysis in material science and biomedical research, J. Radioanal. Nucl. Chem. 279 (3) (2009) 833–846, http://dx.doi.org/10.1007/s10967-008-7386-1.

[2] M. Grdeń, Non-classical applications of chemical analysis based on nuclear activation, J. Radioanal. Nucl. Chem. 323 (2) (2019) 677–714, http://dx.doi.org/10.1007/s10967-019-06977-w.

[3] J.-V. Kratz, Nuclear and Radiochemistry, Wiley, 2021, http://dx.doi.org/10.1002/9783527831944.

[4] A. Türler, V. Pershina, Advances in the production and chemistry of the heaviest elements, Chem. Rev. 113 (2) (2013) 1237–1312, http://dx.doi.org/10.1021/cr3002438.

[5] E. Crouch, Fission-product yields from neutron-induced fission, At. Data Nucl. Data Tables 19 (5) (1977) 417–532, http://dx.doi.org/10.1016/0092-640x(77)90023-7.

[6] S. Amiel, H. Feldstein, Odd-even systematics in neutron fission yields of ^{233}U and ^{235}U, Phys. Rev. C 11 (3) (1975) 845–858, http://dx.doi.org/10.1103/physrevc.11.845.

[7] V.E. Viola, K. Kwiatkowski, M. Walker, Systematics of fission fragment total kinetic energy release, Phys. Rev. C 31 (4) (1985) 1550–1552, http://dx.doi.org/10.1103/physrevc.31.1550.

[8] W.E. Grummitt, G. Wilkinson, Fission products of ^{235}U, Nature 158 (4005) (1946) 163, http://dx.doi.org/10.1038/158163a0.

[9] H. Wollnik, Principles behind a He-jet system and its application for isotope separation, Nucl. Instrum. Methods 139 (1976) 311–318, http://dx.doi.org/10.1016/0029-554x(76)90691-1.

[10] E.E. Tereshatov, M. Semelová, K. Čubová, P. Bartl, M. Němec, J. Štursa, V. Zach, C.M. Folden, J.P. Omtvedt, J. John, Valence states of cyclotron-produced thallium, New J. Chem. 45 (7) (2021) 3377–3381, http://dx.doi.org/10.1039/d0nj05198e.

[11] H. Gäggeler, D. Jost, U. Baltensperger, A. Weber, A. Kovacs, D. Vermeulen, A. Türler, OLGA II, an on-line gas chemistry apparatus for applications in heavy element research, Nucl. Instrum. Methods Phys. Res., Sect. A 309 (1–2) (1991) 201–208, http://dx.doi.org/10.1016/0168-9002(91)90103-w.

[12] Y. Nai-Qi, D.T. Jost, U. Baltensperger, H.W. Gäggeler, The Saphir gas-jet and a first application to an on-line separation of niobium, Radiochim. Acta 47 (1) (1989) 1–8, http://dx.doi.org/10.1524/ract.1989.47.1.1.

[13] W. Fischer, SINQ – the spallation neutron source, a new research facility at PSI, Phys. B: Condens. Matter 234–236 (1997) 1202–1208, http://dx.doi.org/10.1016/s0921-4526(97)00260-3.

[14] D. Jost, E. Lehmann, D. Piguet, M. Gehri, P. Frutiger, M. Pomplun, A. Fleischmann, The new SINQ gas-jet facility, in: Annual Report 1997, Paul Scherrer Institut, Villigen, Switzerland, 1998, p. 20.

[15] M. Wachsmuth, B. Eichler, L. Tobler, D. Jost, H.W. Gäggeler, M. Amman, On-line gas-phase separation of short-lived bromine nuclides from precursor selenium, Radiochim. Acta 88 (12) (2000) http://dx.doi.org/10.1524/ract.2000.88.12.873.

[16] M. Wachsmuth, B. Eichler, L. Tobler, F. Hänssler, H.W. Gäggeler, M. Ammann, Chemical characterization of short-lived selenium and their daughter isotopes from thermal neutron induced fission of ^{235}U at a gas-jet facility, J. Radioanal. Nucl. Chem. 254 (1) (2002) 201–208, http://dx.doi.org/10.1023/a:1020878506388.

[17] C. Düllmann, B. Eichler, R. Eichler, H. Gäggeler, D. Jost, U. Kindler, D. Piguet, S. Soverna, P. Thörle, N. Trautmann, A. Türler, Miss Piggy, a californium-252 fission fragment source as a generator of short-lived radionuclides, Nucl. Instrum. Methods Phys. Res., Sect. A 512 (3) (2003) 595–605, http://dx.doi.org/10.1016/s0168-9002(03)01932-6.

[18] E. Lehmann, Betätigung des Strahlverschlusses des Gas-Jets im Strahlkanal 62 der SINQ zur Dosierung des Neutronenflussniveaus auf den Spaltfolien, Technical Report, Paul Scherrer Institut, Villigen, Switzerland, 1996.

[19] Mirion Technologies (Canberra), Inc., Genie 2000 Gamma acquisition & analysis, V3.3, 2013, URL https://www.mirion.com/products/genie-2000-basic-spectroscopy-software.

[20] J.F. Ziegler, SRIM – the stopping and range of ions in matter, 2013, URL http://www.srim.org/.

[21] J. King, R. Yanez, W. Loveland, J.S. Barrett, J.S. Barrett, B. Oscar, N. Fotiades, F. Tovesson, H.Y. Lee, The total kinetic energy release in the fast neutron-induced fission of ^{232}Th, Eur. Phys. J. A 53 (12) (2017) http://dx.doi.org/10.1140/epja/i2017-12436-9.

[22] D. Wittwer, F. Abdullin, N. Aksenov, Y. Albin, G. Bozhikov, S. Dmitriev, R. Dressler, R. Eichler, H. Gäggeler, R. Henderson, S. Hübener, J. Kenneally, V. Lebedev, Y. Lobanov, K. Moody, Y. Oganessian, O. Petrushkin, A. Polyakov, D. Piguet, P. Rasmussen, R. Sagaidak, A. Serov, I. Shirokovsky, D. Shaughnessy, S. Shishkin, A. Sukhov, M. Stoyer, N. Stoyer, E. Tereshatov, Y. Tsyganov, V. Utyonkov, G. Vostokin, M. Wegrzecki, P. Wilk, Gas phase chemical studies of superheavy elements using the dubna gas-filled recoil separator – stopping range determination, Nucl. Instrum. Methods Phys. Res., Sect. B 268 (1) (2010) 28–35, http://dx.doi.org/10.1016/j.nimb.2009.09.062.

[23] P. Sigmund, A. Schinner, The Bloch correction, key to heavy-ion stopping, J. Appl. Phys. 128 (10) (2020) 100903, http://dx.doi.org/10.1063/5.0015478.

[24] A. Mangiarotti, M. Lopes, M. Benabderrahmane, V. Chepel, A. Lindote, J.P. da Cunha, P. Sona, A survey of energy loss calculations for heavy ions between 1 and 100kev, Nucl. Instrum. Methods Phys. Res., Sect. A 580 (1) (2007) 114–117, http://dx.doi.org/10.1016/j.nima.2007.05.048.

[25] B. Singh, Nuclear data sheets for A=89, Nucl. Data Sheets 85 (1) (1998) 1–170, http://dx.doi.org/10.1006/ndsh.1998.0019.

[26] A. Sonzogni, Nuclear data sheets for A=138, Nucl. Data Sheets 98 (3) (2003) 515–664, http://dx.doi.org/10.1006/ndsh.2003.0004.

[27] D.A. Brown, ENDF/B-VIII.0: THE 8th major release of the ENDF/B library containing cielo-project evaluations, new standards and thermal scattering data, 2018, URL https://www.osti.gov/biblio/1478739.

[28] B. Singh, A.A. Rodionov, Y.L. Khazov, Nuclear data sheets for A=135, Nucl. Data Sheets 109 (3) (2008) 517–698, http://dx.doi.org/10.1016/j.nds.2008.02.001.

[29] N. Nica, Nuclear data sheets for A=140, Nucl. Data Sheets 154 (2018) 1–403, http://dx.doi.org/10.1016/j.nds.2018.11.002.

[30] D. Abriola, M. Bostan, S. Erturk, M. Fadil, M. Galan, S. Juutinen, T. Kibédi, F. Kondev, A. Luca, A. Negret, N. Nica, B. Pfeiffer, B. Singh, A. Sonzogni, J. Timar, J. Tuli, T. Venkova, K. Zuber, Nuclear data sheets for A=84, Nucl. Data Sheets 110 (11) (2009) 2815–2944, http://dx.doi.org/10.1016/j.nds.2009.10.002.

[31] A. Sonzogni, Nuclear data sheets for A=134, Nucl. Data Sheets 103 (1) (2004) 1–182, http://dx.doi.org/10.1016/j.nds.2004.11.001.

[32] S. Bolisetty, R. Mezzenga, Amyloid-carbon hybrid membranes for universal water purification, Nature Nanotechnol. 11 (4) (2016) 365–371, http://dx.doi.org/10.1038/nnano.2015.310.

[33] G. Tiebel, S. Bolisetty, R. Eichler, L. Melnik, R. Mezzenga, P. Steinegger, Removal of ^{235}U fission products from contaminated water using a whey-protein-based activated charcoal hybrid filter material, in: Annual Report 2021, Paul Scherrer Institut, Villigen, Switzerland, 2022, p. 9.

[34] K. Ooe, M.F. Attallah, M. Asai, N. Goto, N.S. Gupta, H. Haba, M. Huang, J. Kanaya, Y. Kaneya, Y. Kasamatsu, Y. Kitatsuji, Y. Kitayama, K. Koga, Y. Komori, T. Koyama, J.V. Kratz, H.V. Lerum, S. Miyashita, Y. Oshimi, V. Pershina, D. Sato, T.K. Sato, Y. Shigekawa, A. Shinohara, A. Tanaka, A. Toyoshima, K. Tsukada, S. Tsuto, T. Yokokita, A. Yokoyama, J.P. Omtvedt, Y. Nagame, M. Schädel, Development of a new continuous dissolution apparatus with a hydrophobic membrane for superheavy element chemistry, J. Radioanal. Nucl. Chem. 303 (2) (2014) 1317–1320, http://dx.doi.org/10.1007/s10967-014-3469-3.